



# First-principles thermodynamic study of the electrochemical stability of Pt nanoparticles in fuel cell applications



Joon Kyo Seo<sup>a</sup>, Abhishek Khetan<sup>b</sup>, Min Ho Seo<sup>a</sup>, Hasuck Kim<sup>a</sup>, Byungchan Han<sup>a,\*</sup>

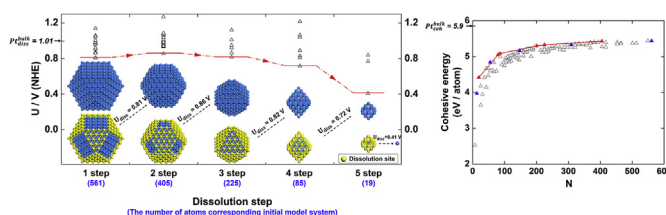
<sup>a</sup> Department of Energy Systems Engineering, DGIST, 50-1 Sang-ri, Hyeonpung-myeon, Dalseong-gun, Daegu 711-873, South Korea

<sup>b</sup> Institut für Technische Verbrennung, RWTH Aachen University, Templergraben 64, 52062 Aachen, Germany

## HIGHLIGHTS

- Ab-initio DFT studies on the electrochemical stability of Pt nanoparticles.
- Evaluation of size and morphology dependent dissolution mechanism in acidic media.
- Identification of the key parameters for the dissolution mechanism.
- Atomistic level pictures of intermediate structures appearing at dissolution step.
- First principles computational message on how to design stable nanocatalysts.

## GRAPHICAL ABSTRACT



## ARTICLE INFO

### Article history:

Received 22 December 2012

Received in revised form

11 March 2013

Accepted 13 March 2013

Available online 26 March 2013

### Keywords:

First-principles calculations

Fuel cell

Nanocatalyst

Degradation mechanism

## ABSTRACT

The durability of Pt-based nanocatalysts in acidic media is one of the key issues hindering the development of efficient fuel cell cathodes, and the factors affecting the durability are not well-understood. In this study, first-principles calculations are used to analyze the electrochemical degradation of Pt nanoparticles. Model systems of Pt nanoparticles in different sizes are designed to calculate the dissolution potentials of these systems. Based strictly on thermodynamics, the results point toward strongly size-dependent dissolution behavior for Pt nanoparticles, the properties of which become similar to that of bulk Pt at diameters larger than 3 nm. Remarkably, the dissolution proceeds through the exposure of more (111) facets at the expense of atoms located at edges, vertices and (111) facets. The size-dependent trends in the dissolution potentials indicate that the competition between two thermodynamic factors, the cohesive energy and the surface energy, determines the dissolution pathway. Based on the findings, several characteristics are proposed that can serve in the rational design of model Pt nanocatalysts.

© 2013 Elsevier B.V. All rights reserved.

## 1. Introduction

The Proton Exchange Membrane (PEM) fuel cell is considered to be one of the key technologies for the generation of clean and environmentally friendly energy [1]. Since fuel cells first served as power sources for spaceflights in the Gemini space program in the

1960s, they have been studied extensively as replacements for conventional fossil fuels for transportation vehicles. Several long-standing issues, such as the high cost of the precious metal-based catalyst and sluggish Oxygen Reduction Reaction (ORR) rates at the cathode, are still a major impediment to widespread commercialization of fuel cells [2–4]. Over the last several decades, experimental and computational studies have focused on the utilization of nanoscale Pt particles as novel functional catalysts primarily because of their high surface-to-volume ratio [5–7]. Indeed, many pure and Pt-based alloy nanoparticles have been identified to

\* Corresponding author. Tel.: +82 53 785 6412; fax: +82 53 785 6409.

E-mail address: [hanbc@dgist.ac.kr](mailto:hanbc@dgist.ac.kr) (B. Han).

be materials that show substantially improved catalytic activities [8–10].

Recent reports, however, indicate that the structural integrity of Pt nanoparticles is severely compromised in acidic media; this lack of structural integrity reduces the durability of the fuel cell to unacceptable levels [11–15]. Several mechanisms underlying the degradation phenomena have been proposed: direct electrochemical dissolution of the metal into the acidic electrolyte [16–20], oxide formation and subsequent dissolution [21–24], pseudo-Ostwald ripening (dissolution of the catalyst into the electrolyte and redeposition to form larger particles) [11–15] and corrosion of the support materials [25–29]. Depending on the operating conditions and the topology of the catalyst layers at the cathode, one mechanism or a combination of these mechanisms in parallel may drive the degradation [17].

The direct electrochemical dissolution of catalyst atoms in acidic media is especially interesting because it has been found to be the most predominant degradation mechanism [16–20] although in the bulk form, Pt is chemically the noblest metal. A comprehensive picture, however, of the properties of the catalyst that affect the dissolution behavior of the catalyst at the atomic scale is still missing. Experimental observations combined with Density Functional Theory (DFT) calculations have shown that if Pt nanoparticles smaller than 2 nm are exposed to acidic media, they disappear from an Au support on a short time scale [19]; whereas other studies propose that the  $\text{Pt}^{2+}$  ions in the acidic electrolyte primarily come from the stepwise atomic dissolution of the outermost shell [21].

An accurate understanding of the electrochemical degradation process at the atomic scale is an important step toward the development of functional, high-durability catalysts. The potential at which a material may undergo partial or complete dissolution, designated the dissolution potential throughout the rest of this paper, is a good indicator of the material's resistance against electrochemical degradation [19]. In this work, first-principles DFT calculations are utilized extensively to search for the thermodynamically most plausible dissolution path by calculating the dissolution potential as a function of the size of the Pt nanoparticle. Section 2 of the text describes the assumptions made in the study and the method used to design the different-sized nanoparticles, which are subsequently analyzed through simulations. In Sections 3 and 4, the computational approach for the DFT calculations and the theoretical formulation for calculating the dissolution potentials are described. The results and their implications for the rational design of catalysts are discussed in Section 5; a summary of the limitations of the present model follows in Section 6.

## 2. Model systems

Four model systems of Pt nanoparticles of different sizes:  $\text{Pt}_{55}$  (55 atoms and 1.1 nm in diameter),  $\text{Pt}_{147}$  (147 atoms and 1.6 nm in diameter),  $\text{Pt}_{309}$  (309 atoms and 2.2 nm in diameter) and  $\text{Pt}_{561}$  (561 atoms and 2.7 nm in diameter), were setup to be the starting points

for DFT calculations, as shown in Fig. 1. The size of a nanoparticle was defined to be the distance between two diametrically opposite vertices in this work. The shape of the nanoparticle was chosen to be an ideal cubo-octahedron structure, consisting of solely (111) and (100) facets; this shape results in an optimal configuration with minimal total energy for a given particle size [30–32]. The cubo-octahedron structure has often been observed experimentally in nanoscale catalysts for fuel cell applications [33–35]. Although this structure is relatively stable, its formation can be hindered by unfavorable kinetic or activation requirements that depend on the particle size [36]. This factor is outside of the scope of the present study.

The dissolution potential of an individual atom in the Pt nanoparticle may depend on the local coordination number and geometry of the atom. Hence, four types of symmetrically inequivalent atomic sites on the outermost shell, namely: vertex, edge, and the (100) and (111) facets, as shown in Fig. 1, were identified. Atomic sites belonging to a given type were then grouped together; thus, this grouping resulted in four basic dissolution candidates with atoms that could be subjected to simultaneous dissolution because of the atoms nearly symmetric locations on the surface of the nanoparticle, as shown in Fig. 2(a–d). It should be noted that the minor local asymmetry within each edge, (100) and (111) site has been neglected because these sites have almost identical coordination environments. Furthermore, various combinations of these four basic candidates resulted in several other possible candidates for dissolution with inequivalent atomic sites, as shown in Fig. 2(e–o); these candidates could be subjected to simultaneous dissolution.

The first dissolution step for a nanoparticle of a given size was imagined to take place in such a way that during the process, all the yellow atoms (in web version) of the dissolution candidates of the nanoparticle, as shown in Fig. 2, were removed simultaneously. The dissolution potential for such a step was calculated for each candidate separately with first-principles DFT. Because the dissolution potential is a measure of the resistance against electrochemical degradation, the most viable path for the dissolution was suitably chosen to occur, at each step, through the candidate that had the lowest evaluated dissolution potential. After completion of a dissolution step, the resultant structure was then selected to be the initial model system for the next step, and several possible dissolution candidates for this new model system were again identified with the same methodology as described above. This process was repeated until a single atom remained; thus, this process unveiled the most thermodynamically viable pathway to the complete dissolution of the nanoparticle.

## 3. Computational details

The Generalized Gradient Approximation (GGA) [37] by Perdew, Burke and Ernzerhof (PBE) [38], as implemented in the Vienna Ab-initio Simulation Package (VASP) [37], was used to describe the exchange-correlation energies of the electrons. Pseudo-potentials

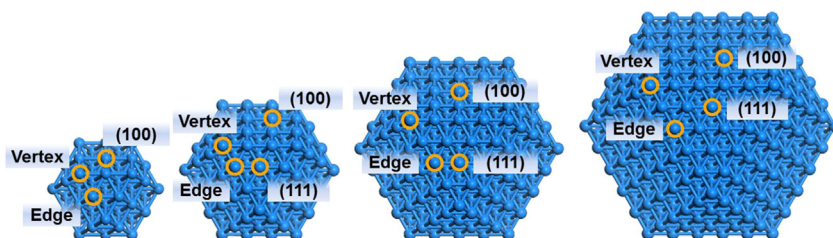


**Fig. 1.** Model systems of Pt nanoclusters (1.1, 1.6, 2.2 and 2.7 nm in diameter). Symmetrically inequivalent atomic sites on the outermost shells are marked with circles according to their local environments.

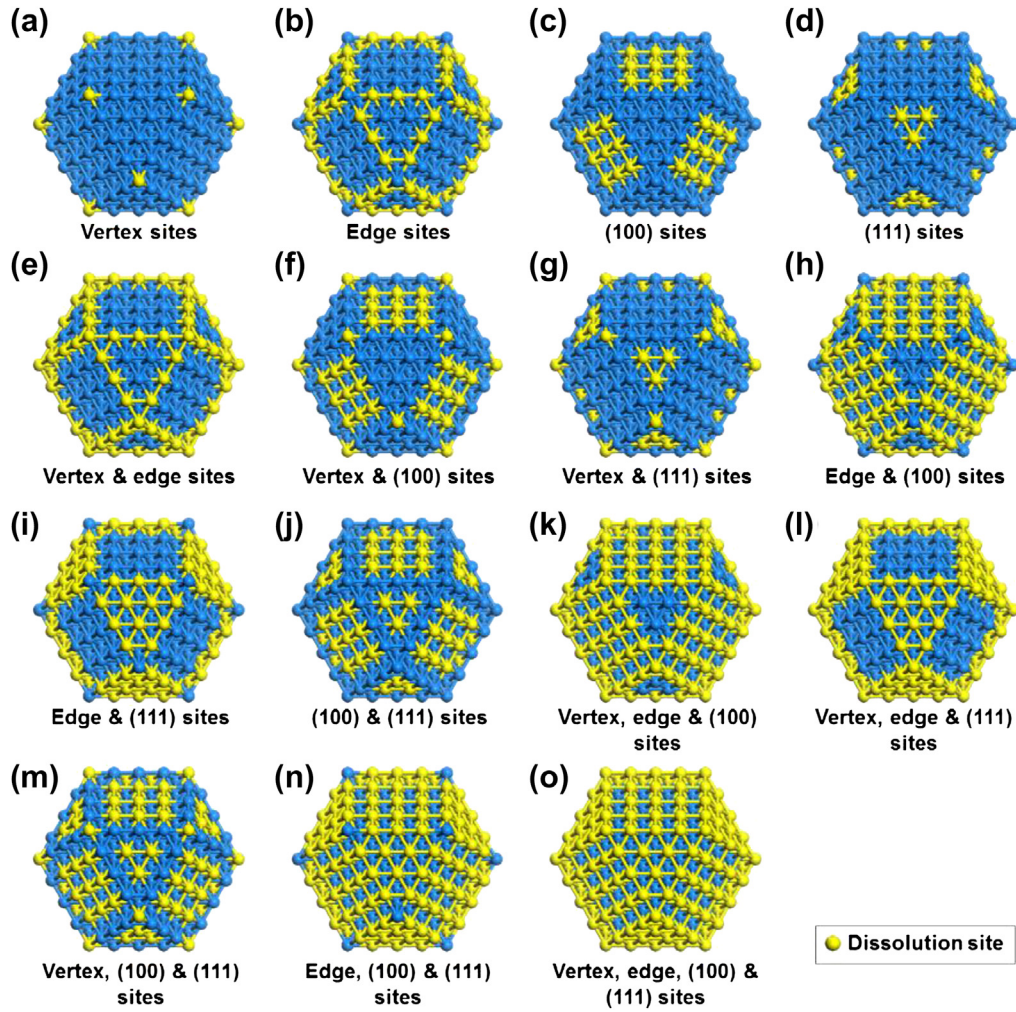
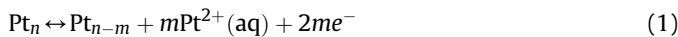


Fig. 2. Dissolution candidates of the outermost shell (diameter of model system: 2.2 nm).

generated through the Projector Augmented Wave (PAW) method [39,40] were used to replace the interaction potentials of the core electrons. A gamma point mesh with  $1 \times 1 \times 1$   $k$ -points was specified in the Brillouin zone, and periodic boundary conditions were imposed on the model systems with a vacuum space that was twice as thick as the cluster size to prohibit interactions among the images. All the atoms were fully relaxed to calculate the optimized structure of each nanoparticle with a cutoff energy of 325 eV on a plane wave basis set. The calculated lattice constant for bulk fcc Pt metal was found to be 3.98 Å in this work; this value agrees well with the experimentally measured value of 3.92 Å [41].

#### 4. Theoretical formalism for the dissolution potential

It has been proposed [16–20] that Pt nanoparticles degrade electrochemically through the direct dissolution of surface atoms into the surrounding acidic media, as given by Eq. (1)



where  $\text{Pt}_n$  and  $\text{Pt}_{n-m}$  are the nanoparticles consisting of  $n$  and  $n - m$  Pt atoms, respectively. Eq. (1) describes a reversible reaction in which  $m$  atoms on the outermost shell of the Pt nanoparticle are ionized to  $\text{Pt}^{2+}$ , and the dissolution potential of the nanoparticle is calculated with Eq. (2), with respect to the Standard Hydrogen Electrode (SHE)

$$U_m = \frac{1}{2me} \{E(\text{Pt}_{n-m}) - E(\text{Pt}_n)\} + \frac{1}{2e} \left\{ \mu^0(\text{Pt}^{2+}, \text{aq}) + kT \log_e(a_{\text{Pt}^{2+}}) \right\} \quad (2)$$

where  $E$  indicates the total energy calculated by DFT and  $\mu^0$ ,  $k$ ,  $T$ ,  $a_{\text{Pt}^{2+}}$  have their usual definitions: the chemical potential of the  $\text{Pt}^{2+}$  ions at standard conditions, the Boltzmann constant, the absolute temperature and the activity of the  $\text{Pt}^{2+}$  ions, respectively. Instead of the difficult calculation of the ionic solvation energy of the  $\text{Pt}^{2+}$  ions ( $\mu^0(\text{Pt}^{2+}, \text{aq})$ ) from first principles [42], the electrochemical dissolution reaction of bulk Pt, given by Eq. (3), is employed.



The dissolution potential of bulk Pt in Eq. (3) is given by

$$U_{\text{bulk}} = \frac{1}{2e} \left\{ \mu^0(\text{Pt}^{2+}, \text{aq}) + kT \log_e(a_{\text{Pt}^{2+}}) - E(\text{Pt}_{\text{bulk}}) \right\} \quad (4)$$

where  $U_{\text{bulk}}$  is known to be 1.011 V (relative to a SHE) [43] if the concentration of  $[\text{Pt}^{2+}]$  is  $10^{-6}$  M [19]. The calculations in this work show that the energy per atom of bulk Pt ( $E(\text{Pt}_{\text{bulk}})$ ) is  $-6.03$  eV. Through Eqs. (2) and (4),  $U_m$  is expressed by

$$U_m = U_{\text{bulk}} + \frac{1}{2me} \{E(\text{Pt}_{n-m}) + mE(\text{Pt}_{\text{bulk}}) - E(\text{Pt}_n)\} \quad (5)$$

$U_m$  was calculated with DFT for each of the dissolution candidates of the four model systems and for the candidates of subsequent structures that were encountered during the most thermodynamically viable dissolution path.

## 5. Results and discussion

The dissolution potentials for each of the four model systems and for the subsequently appearing structures, were calculated through the formalism described earlier. Fig. 3 shows the dissolution potentials,  $U_m$ , of the Pt nanoparticles as a function of the size of the particles. Fig. 3(a) shows the dissolution pathway for the Pt nanoparticle that is 2.7 nm in size and is composed of 561 atoms. For each dissolution step, several dissolution candidates were systematically considered and their dissolution potentials were

evaluated. The calculated dissolution potentials were plotted as a function of the size of the initial model system for that step. The candidate with the lowest dissolution potential was selected for simultaneous removal of the atomic sites marked in yellow in Fig. 3. The nanocluster thus obtained served as the initial model system for the next dissolution step. The numbers for each step in Fig. 3(a) represent the number of atoms in the nanoparticle that served as the initial model system for that dissolution step. The procedure was continued until a single atom remained. The red line, which is constructed by joining the points that correspond to the lowest dissolution potentials, denotes the most thermodynamically viable path for step-by-step dissolution. A similar methodology was employed to construct the plots for other model systems. The results from this work indicate that Pt nanoclusters with sizes smaller than approximately 3 nm have electrochemical stabilities weaker

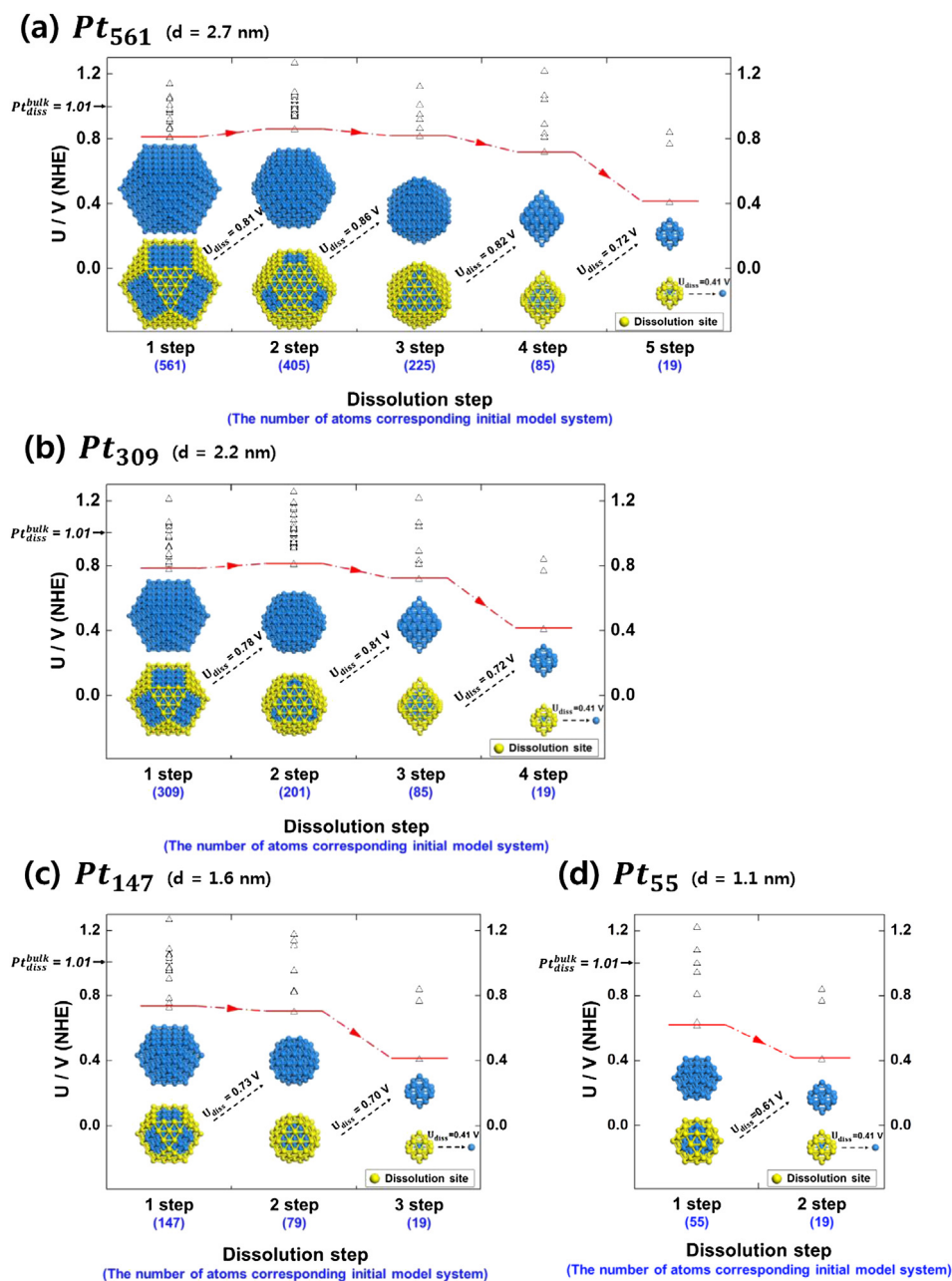


**Fig. 3.** The electrochemical dissolution of the nanoparticle (diameters of model systems: 2.7, 2.1, 1.6 and 1.1 nm).  $\Delta$  represents the ab-initio calculated dissolution potential of the dissolution candidates for each nanoparticle (upper illustration). The red solid line indicates the lowest dissolution potential if particular atoms (yellow color in lower illustration) dissolve. (For interpretation of the references to color in this figure legend, the reader is referred to the web version of this article.)

than that of bulk Pt (1.01 V relative to a SHE); this result is in agreement with previous reports [19].

Note that at each dissolution step, the dissolution proceeds in a manner such that the structures that emerge after dissolution reveal a larger fraction of atoms on the outermost shell that belong to (111) facets, at the expense of atoms located at edges, vertices and (111) facets. For example, for the Pt nanocluster composed of 561 atoms (approximately 2.7 nm), the 1st dissolution step, which removes the atoms marked in yellow, results in an increased fraction of the surface area that is covered by the (111) planes; thus, this step leads to a truncated-octahedron structure composed of 405 atoms. It is not surprising that this characteristic of the dissolution mechanism is evident across all the model systems because the presence of a larger fraction of (111) facets leads to a relatively more stable nanoparticle. The (111) facet is rigorously known to be the most stable of all the extended Pt surfaces and has the lowest surface energy [44,45].

Remarkably, for model systems Pt<sub>561</sub> (Fig. 3(a)) and Pt<sub>309</sub> (Fig. 3(b)), the dissolution potential along the thermodynamically most viable path (red line) at the second step increases to a value slightly greater than the value at the first step. This result indicates that for these two cases, the nanoparticle obtained after the first step is more durable than the model system itself, possibly because of the increase in the fraction of the stabilizing (111) facet. These values, however, subsequently decrease rapidly as the nanoparticle size decreases. Thus, one finds that in addition to the surface energy, the thermodynamics of the dissolution mechanism are also clearly influenced by the size of the nanoparticle.

We propose that at least two thermodynamic factors control the electrochemical dissolution process. A subtle interplay between the size-dependent cohesive energy (per atom) and the surface energy energetically stabilizes the Pt nanoparticle. At each dissolution step, the surface energy is minimized as much as the other constraints, such as the strain on the shell, and simultaneously the cohesive energy (per atom) decreases because of the decreasing size of the nanoparticle. Although lower surface energies increase the stability, lower cohesive energies (per atom) decrease the stability of the nanoparticle. It has already been proposed that insufficient cohesive energy is a major driving force behind the electrochemical degradation of Pt nanoparticles through dissolution into acidic solution [19,46]. Nevertheless, a detailed study and analysis of how the structures evolve during the dissolution process, and of the factors influencing this evolution, is not yet available in the current literature.

To understand the evolution of the nanoparticle structures in greater detail, the cohesive energies of the Pt nanoparticles were calculated from first principles as a function of the size (or interchangeably, as a function of the total number of atoms in the cluster,  $N$ ) and were plotted, as shown in Fig. 4. The cohesive energy per atom decreases dramatically as the size decreases below approximately 250 atoms. For nanoparticles larger than approximately 250 atoms in size, a slowly decay of the cohesive energy can be observed as size decreases. In this region, the stabilizing effect of the increasing fraction of (111) surface area is dominant. This interplay certainly explains the slight increases in the dissolution potentials after the first step for the Pt<sub>561</sub> and Pt<sub>309</sub> model systems. For nanoparticles smaller than these sizes, the stabilizing effect of the increased fraction of (111) surface is overpowered by the rapidly destabilizing effect of the cohesive energy. Thus, the dissolution potential for these nanoparticles decreases with their size. We propose that it is the size-dependent competition between these two factors that dictates the most thermodynamically viable mechanism. The influence of these factors is reflected well by the calculated results.

Furthermore, the thermodynamic dissolution path identified here agrees well with the red line that denotes the reverse cohesive

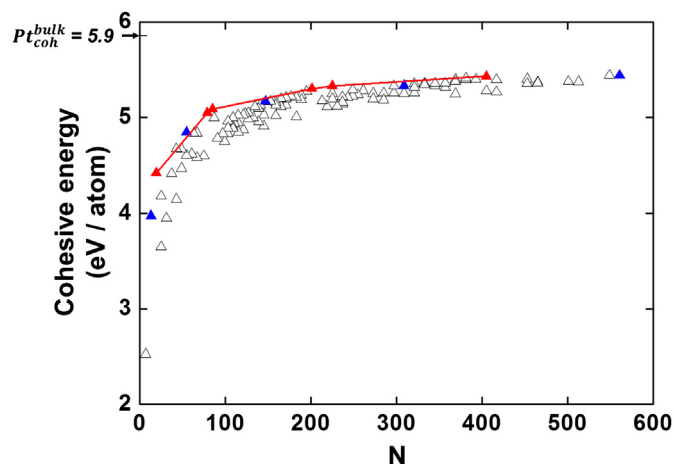


Fig. 4. Cohesive energy of the nanoparticle as a function of the number of atoms. Triangles represent the ab-initio calculated cohesive energy per atom; the blue triangles are the model systems, and the red triangles are the intermediate structures that appear in the viable dissolution path. The red line denotes the upper limit of the calculated cohesive energies for the intermediate structures. (For interpretation of the references to color in this figure legend, the reader is referred to the web version of this article.)

energy convex hull, shown in Fig. 4. This observation is succinctly represented by the red triangles on this line; these triangles correspond to the intermediate structures encountered in the most thermodynamically viable dissolution paths for all the model systems. The red line shows the upper limit of the calculated cohesive energies and indicates the most stable scenarios for a given particle size. Remarkably, the nanoparticles corresponding to these red triangles are quite similar to the closely packed “magic number” nanoclusters, which have also been found to be relatively stable [47,48].

The results from this work create the groundwork for the conceptual design with minimal material cost of highly durable Pt catalysts; this design may be achieved with novel methodologies that expose more (111) planes on the outermost shell [49,50] for particle sizes larger than 3 nm.

It has been previously reported that the (100) Pt facets contribute to the ORR activity much less than the (111) Pt facets [51]. The evidence for the Pt (111) facet being more active toward ORR may also be found in another experimental study that calls this selectivity of electrochemical reactions with respect to the type of facet “structural sensitivity” [52]. Hence, we believe that designing Pt nanoparticles with a high fraction of (111) planes and minimal (100) planes to accommodate the strain field may be a rational way to satisfy the ORR activity and electrochemical durability issues.

## 6. Limitations of our model

In the present work, the most viable electrochemical dissolution path was identified by considering only the thermodynamics of the process, and the effects of some crucial factors, such as kinetics, support effects, other degradation mechanisms, etc., were excluded. First, one must consider the overall fuel cell cathode where the degradation process takes place; additional factors such as the amount of catalyst loading, the temperature, the pressure, the pH of the solution, the solvation and passivation of the surface and the electrochemical double layer influence the degradation behavior. The aim of this study, however, is to investigate those properties inherent to the nanocatalyst that influence degradation of the nanocatalyst.

If the thermodynamic driving force is sufficient to overcome any kinetic activation requirements, the arguments presented in this paper hold well. This assumption implies that the Pt atoms are

mobile at each dissolution step to reconstruct the nanoparticle and form the thermodynamically most stable configuration. The central assumption of this work is the consideration of only one mechanism of degradation i.e., dissolution into acidic media. It can be argued that this assumption holds reasonably well for the range of nanoparticle sizes that have been studied. Experimental evidence indicates that for nanoparticles 1–4 nm in diameter, electrochemical dissolution is the primary mechanism [16,19,20,53,54]. In addition, other possible mechanisms of degradation such as Ostwald ripening, support corrosion and Pt redeposition have not been considered in the present work. The Ostwald ripening mechanism comprises sub-processes such as dissolution, transport and coalescence [11–15]. Because this study considers the degradation of individual nanoparticles and not groups of nanoparticles, the ripening mechanism has much less relevance to the present work. Furthermore, this process has been found to be essentially independent of the particle size distribution [55]. This work also assumes the simultaneous dissolution of many atomic sites in a uniform manner; this assumption may not be true because in reality, the atoms may dissociate from the nanoparticle individually. It has been suggested in experimental findings, however, that the degradation process takes place through layer-by-layer dissolution of the (111) facets [21].

In addition, the model systems do not incorporate the effect of the support. This lack of incorporation does not imply that support effects are negligible or unimportant; however, the dependence of the energetics of the dissolution process on the properties of the nanoparticle alone is better revealed by the approach adopted here. Recently, it has been reported that several oxide support materials can enhance the electrochemical durability of Pt nanoparticles [56]. As such, the dissolution potentials for supported nanoparticles could be higher in fuel cell operation.

## 7. Conclusions

In this work, ab-initio thermodynamics have been used to understand the evolution of nanoparticle morphologies and the factors that affecting this evolution during the electrochemical dissolution process. The findings of this study lead to several remarkable observations. It is observed that, irrespective of the size of the nanoparticle, the mechanism proceeds at each step by exposing more (111) facets at the expense of atoms located at edges, vertices and (111) facets. In contrast, a strongly size-dependent behavior is observed for the dissolution potential, especially for smaller sized nanoparticles; this behavior can be attributed to the strong decay in the cohesive energy as size decreases. Based on the emerging trends for the values of dissolution potentials, it can be concluded that the overall mechanism is dictated by the competition between the stabilizing effect of the increasing fraction of (111) surface area on the outermost shell and the destabilizing effect because of the decreasing cohesive energy. The intermediate structures encountered for all the model systems are found to lie on the upper limit of the cohesive energy values that correspond to a given nanoparticle size; thus, this result indicates that the structures are relatively stable nanoparticles. Moreover, these structures are found to be notably similar to the magic number clusters that are known for their relatively high stability. In totality, the arguments presented in this study are well-founded and make a strong case for the thermodynamically driven mechanism assumed at the beginning of the study.

## Acknowledgments

This work was supported by New and Renewable Energy R&D Program (20113020030020) under the Ministry of Knowledge

Economy, Republic of Korea. The authors also thank DGIST for providing research funding through the DGIST R&D Program of the Ministry of Education, Science and Technology of Korea (12-BD-0102). This work was supported in part by the IT R&D Program of MKE/KEIT (10041856). The Korea Institute of Science and Technology Information (KISTI) generously allowed us to use the supercomputing facility (KSC-2012-C2-66).

## References

- [1] L. Carrette, K.A. Friedrich, U. Stimming, *ChemPhysChem* 1 (2000) 162–193.
- [2] U.S. Department of Energy, Energy Efficiency and Renewable Energy, The Fuel Cell Technologies Office Multi-year Research, Development and Demonstration Plan. [www1.eere.energy.gov/hydrogenandfuelcells/mypp/pdfs/fuel\\_cells.pdf](http://www1.eere.energy.gov/hydrogenandfuelcells/mypp/pdfs/fuel_cells.pdf), (last accessed 22.02.13).
- [3] M.K. Debe, *Nature* 486 (2012) 43–51.
- [4] F.T. Wagner, B. Lakshmanan, M.F. Mathias, *J. Phys. Chem. Lett.* 1 (2010) 2204–2219.
- [5] J. Greeley, I.E.L. Stephens, A.S. Bondarenko, T.P. Johansson, H.A. Hansen, T.F. Jaramillo, J. Rossmeisl, I. Chorkendorff, J.K. Nørskov, *Nat. Chem.* 1 (2009) 552–556.
- [6] H.A. Gasteiger, N.M. Markovic, *Science* 324 (2009) 48–49.
- [7] V.R. Stamenkovic, B. Fowler, B.S. Mun, G. Wang, P.N. Ross, C.A. Lucas, N.M. Markovic, *Science* 315 (2007) 493–497.
- [8] P. Strasser, S. Koh, T. Anniyev, J. Greeley, K. More, C. Yu, Z. Liu, S. Kaya, D. Nordlund, H. Ogasawara, M.F. Toney, A. Nilsson, *Nat. Chem.* 2 (2010) 454–460.
- [9] K.A. Kuttitzi, K. Sasaki, Y. Choi, D. Su, P. Liu, R.R. Adzic, *Energy Environ. Sci.* 5 (2012) 5297–5304.
- [10] J.X. Wang, H. Inada, L. Wu, Y. Zhu, Y. Choi, P. Liu, W.-P. Zhou, R.R. Adzic, *J. Am. Chem. Soc.* 131 (2009) 17298–17302.
- [11] P.J. Ferreira, G.J.L. O', Y. Shao-Horn, D. Morgan, R. Makharia, S. Kocha, H.A. Gasteiger, *J. Electrochem. Soc.* 152 (2005) A2256–A2271.
- [12] Y. Shao-Horn, W.C. Sheng, S. Chen, P.J. Ferreira, E.F. Holby, D. Morgan, *Top. Catal.* 46 (2007) 285–305.
- [13] E.F. Holby, W. Sheng, Y. Shao-Horn, D. Morgan, *Energy Environ. Sci.* 2 (2009) 865–871.
- [14] R. Borup, J. Meyers, B. Pivovar, Y.S. Kim, R. Mukundan, N. Garland, D. Myers, M. Wilson, F. Garzon, D. Wood, *Chem. Rev.* 107 (2007) 3904–3951.
- [15] K. Hartl, M. Hanzlik, M. Arenz, *Energy Environ. Sci.* 4 (2010) 234–238.
- [16] F.J. Perez-Alonso, C.F. Elkjaer, S.S. Shim, B.L. Abrams, I.E. Stephens, I. Chorkendorff, *J. Power Sources* 196 (2011) 6085–6091.
- [17] J.C. Meier, I. Katsounaros, C. Galeano, H.J. Bongard, A.A. Topalov, A. Kostka, A. Karschin, F. Schuth, K.J.J. Mayrhofer, *Energy Environ. Sci.* 5 (2012) 9319–9330.
- [18] I.E. Stephens, A.S. Bondarenko, U. Grönberg, J. Rossmeisl, I. Chorkendorff, *Energy Environ. Sci.* 5 (2012) 6744–6762.
- [19] L. Tang, B. Han, K. Persson, C. Friesen, T. He, K. Sieradzki, G. Ceder, *J. Am. Chem. Soc.* 132 (2010) 596–600.
- [20] L. Tang, X. Li, R.C. Cammarata, C. Friesen, K. Sieradzki, *J. Am. Chem. Soc.* 132 (2010) 11722–11726.
- [21] V. Komanicky, K.C. Chang, A. Menzel, N.M. Markovic, H. You, X. Wang, D. Myers, *J. Electrochem. Soc.* 153 (2006) B446–B451.
- [22] M. Darling, *J. Electrochem. Soc.* 150 (2003) A1523–A1527.
- [23] Y. Sugawara, T. Okayasu, A.P. Yadav, A. Nishikata, T. Tsuru, *J. Electrochem. Soc.* 159 (2012) F779–F786.
- [24] M.H. Seo, E.J. Lim, S.M. Choi, S.H. Nam, H.J. Kim, W.B. Kim, *Int. J. Hydrogen Energy* 36 (2011) 11545–11553.
- [25] S. Maass, F. Finsterwalder, G. Frank, R. Hartmann, C. Merten, *J. Power Sources* 176 (2008) 444–451.
- [26] S. Zhang, X. Yuan, H. Wang, W. Mérida, H. Zhu, J. Shen, S. Wu, J. Zhang, *Int. J. Hydrogen Energy* 34 (2009) 388–404.
- [27] H. Schulenburg, B. Schwanitz, N. Linse, G.N.G. Scherer, A. Wokaun, J. Krbanjevic, R. Grothausmann, I. Manke, *J. Phys. Chem. C* 115 (2011) 14236–14243.
- [28] K. Schlögl, K.J. Mayrhofer, M. Hanzlik, M. Arenz, *J. Electroanal. Chem.* 662 (2011) 355–360.
- [29] Y. Shao, G. Yin, Y. Gao, *J. Power Sources* 171 (2007) 558–566.
- [30] R. Esparza, G. Rosas, M. López Fuentes, J. Sánchez Ramírez, U. Pal, J. Ascencio, R. Pérez, *Mater. Charact.* 58 (2007) 694–700.
- [31] Y. Okamoto, *Chem. Phys. Lett.* 429 (2006) 209–213.
- [32] C. Herring, *Phys. Rev.* 82 (1951) 87–93.
- [33] M. Sattler, P. Ross, *Ultramicroscopy* 20 (1986) 21–28.
- [34] E. Antolini, J. Perez, *J. Mater. Sci.* 46 (2011) 4435–4457.
- [35] K. Kinoshita, *J. Electrochem. Soc.* 137 (1990) 845–848.
- [36] Z. Wang, *J. Phys. Chem. B* 104 (2000) 1153–1175.
- [37] G. Kresse, J. Furthmüller, *Phys. Rev. B* 54 (1996) 11169–11186.
- [38] J.P. Perdew, K. Burke, M. Ernzerhof, *Phys. Rev. Lett.* 77 (1996) 3865–3868.
- [39] P.E. Blochl, *Phys. Rev. B* 50 (1994) 17953–17979.
- [40] G. Kresse, D. Joubert, *Phys. Rev. B* 59 (1999) 1758–1775.
- [41] C. Kittel, *Introduction to Solid State Physics*, eighth ed., Wiley, New York, 2004. (Chapter 1).
- [42] J. Tomasi, B. Mennucci, R. Cammi, *Chem. Rev.* 105 (2005) 2999–3093.
- [43] M. Pourbaix, *Atlas of Electrochemical Equilibria in Aqueous Solutions*, second ed., National Association of Corrosion Engineers, Houston, 1974. (Chapter IV).
- [44] H.L. Skriver, N. Rosengard, *Phys. Rev. B* 46 (1992) 7157.

- [45] L. Vitos, A.V. Ruban, H.L. Skriver, J. Kollar, *Surf. Sci.* 411 (1998) 186–202.
- [46] W.H. Qi, M.P. Wang, *J. Mater. Sci. Lett.* 21 (2002) 1743–1745.
- [47] A.R. Tao, S. Habas, P. Yang, *Small* 4 (2008) 310–325.
- [48] K.J. Klabunde, R.M. Richards, *Nanoscale Materials in Chemistry*, second ed., John Wiley & Sons, Hoboken, 2009. (Part I).
- [49] J. Wu, J. Zhang, Z. Peng, S. Yang, F.T. Wagner, H. Yang, *J. Am. Chem. Soc.* 132 (2010) 4984–4985.
- [50] J. Zhang, H. Yang, J. Fang, S. Zou, *Nano Lett.* 10 (2010) 638–644.
- [51] B. Han, V. Viswanathan, H. Pitsch, *J. Phys. Chem. C* 116 (2012) 6174–6183.
- [52] N.M. Markovic, T.J. Schmidt, V. Stamenkovic, P.N. Ross, *Fuel Cells* 1 (2001) 105–116.
- [53] R. Makharia, S. Kocha, P. Yu, M.A. Sweikart, W. Gu, F. Wagner, H.A. Gasteiger, *ECS Trans.* 1 (2006) 3–18.
- [54] Z. Yang, S. Ball, D. Condit, M. Gummalla, *J. Electrochem. Soc.* 158 (2011) B1439–B1445.
- [55] A.K. Datye, Q. Xu, K.C. Kharas, J.M. McCarty, *Catal. Today* 111 (2006) 59–67.
- [56] S.-Y. Huang, P. Ganesan, S. Park, B.N. Popov, *J. Am. Chem. Soc.* 131 (2009) 13898–13899.